

 Hot Paper


Layered Titanium Sulfide Cathode for All-Solid-State Magnesium Batteries

Lasse N. Skov,^[a] Jakob B. Grinderslev,^[a] and Torben R. Jensen^{*[a]}

Magnesium solid-state batteries attract significant attention as a future mean of energy storage. Here we present the first cathode study of an inorganic all-solid-state magnesium battery using a magnesium metal anode, a nanocomposite electrolyte $\text{Mg}(\text{BH}_4)_2 \cdot 1.6\text{NH}_3\text{-MgO}$ (75 wt %), and a layered titanium disulfide (TiS_2) as cathode active material. The structural transformations of TiS_2 particles with different sizes are investigated at different stages of battery life. Reversible Mg^{2+} intercalation occurs via three structurally distinct phases of Mg_xTiS_2 , identified by powder X-ray diffraction. Magnesium intercalates

initially on octahedral sites and at higher depth of discharge on tetrahedral sites in the interlayers of TiS_2 , which leads to an expansion initially mainly along the c -axis and later along both the a - and c -axes. A maximum discharge capacity of 172 mAh g^{-1} ($\Delta x = 0.36$ in Mg_xTiS_2) is observed for smaller TiS_2 particles. Parasitic reactions could be reduced by decreasing the cut-off voltage by a constant current constant voltage cycling procedure. The chemical diffusion coefficient of the entire cell is found from galvanostatic intermittent titration technique experiments to be in the order of 10^{-15} to $10^{-19} \text{ cm}^2 \text{s}^{-1}$.

Introduction

Batteries are a central technology in the decarbonization of the transport and energy sectors. Currently, state-of-the-art batteries are based on lithium (Li) ions as the charge carrier, but magnesium (Mg) is a promising candidate for cheaper and better batteries. A Mg-metal anode offers a high theoretical capacity (3833 mAh cm^{-3} , 2205 mAh g^{-1}), and has a low standard potential of -2.37 V vs. standard hydrogen electrode (SHE).^[1] In comparison, the anode in commercial Li-ion batteries is Li intercalated in graphite (LiC_6) with a lower specific capacity of 850 mAh cm^{-3} (372 mAh g^{-1}), while another prospective technology based on Li-metal anodes has a capacity of 2062 mAh cm^{-3} (3862 mAh g^{-1}).^[2,3] However, commercialization of Li-metal anodes is challenging due to dendrite formation, which appears to be less pronounced for Mg-metal.^[4] Furthermore, a solid-state electrolyte may increase the overall safety by replacing the liquid/organic electrolyte and the separator in a liquid battery.

Monovalent cationic conduction is well established in the solid state, but a significantly lower mobility is observed for divalent cations, such as Mg^{2+} , due to a higher charge density.^[5,6] High Mg^{2+} ionic conductivity at moderate temperatures, below 60°C , is almost exclusively reported for magne-

sium borohydride derivatives, i.e., $\text{Mg}(\text{BH}_4)_2$ coordinated with different neutral organic ligands such as ammine- or ether-derivatives.^[7–13] Among these, the nanocomposite $\text{Mg}(\text{BH}_4)_2 \cdot 1.6\text{NH}_3\text{-MgO}$ (75 wt %), consisting of the compounds $0.4\text{Mg}(\text{BH}_4)_2 \cdot \text{NH}_3 \cdot 0.6\text{Mg}(\text{BH}_4)_2 \cdot 2\text{NH}_3$ and MgO nanoparticles display a good mechanical stability and high ionic conductivity of $\sigma(\text{Mg}^{2+}) = 5.0 \times 10^{-4} \text{ S cm}^{-1}$ at 60°C .^[10]

The $\text{Mg}(\text{BH}_4)_2 \cdot 1.6\text{NH}_3\text{-MgO}$ (75 wt %) electrolyte displays stable magnesium plating/stripping processes in a symmetric magnesium cell and an oxidative stability of 1.2 V vs. Mg/Mg^{2+} . Thus, on one hand the reducing properties of the tetrahydridoborate anion, BH_4^- , make the electrolyte stable towards a magnesium metal anode, but on the other hand provide limitations on the possible useful cathode materials. The oxidation current at voltages above 1.2 V vs. Mg/Mg^{2+} decreased during extended cycling to 2.5 V , but the magnesium plating/stripping was preserved, suggesting the formation of an ion-conducting and possible favorable interface, which can expand the electrochemical stability window.^[10] However, a full battery cell using this electrolyte remains to be reported. In fact, only one rechargeable magnesium all-solid-state battery cell has been described, using the $\text{Mg}(\text{BH}_4)_2 \cdot 1.5\text{THF}\text{-MgO}$ (75 wt %) as the solid electrolyte, Mg-metal as the anode and layered titanium(IV)sulfide, TiS_2 , as the cathode.^[11]

In general, high capacity cathodes with low migration barriers for divalent metals are challenging to develop, owing to stronger interactions between the cations (M^{2+}) and the anion framework, which often introduces significant structural changes and volume expansion. TiS_2 is a well-studied intercalation cathode for Li-ion batteries,^[14] which has also been investigated with solid-state Li- and Na-electrolytes,^[15–17] and for magnesium batteries using liquid electrolytes. An initial discharge capacity of 270 mAh g^{-1} ($x = 0.56$ in Mg_xTiS_2) with C/20 was reported for a liquid all-phenyl complex in THF cycled at 60°C .^[18] In the subsequent cycles the discharge capacity decreased to around 160 mAh g^{-1} ($x = 0.33$). Another study

[a] Dr. L. N. Skov, Dr. J. B. Grinderslev, Prof. Dr. T. R. Jensen
Interdisciplinary Nanoscience Center (iNANO) and Department of Chemistry,
Aarhus University
Langelandsgade 140, 8000 Aarhus C, Denmark
E-mail: trj@chem.au.dk

 Supporting information for this article is available on the WWW under
<https://doi.org/10.1002/batt.202300185>

 © 2023 The Authors. *Batteries & Supercaps* published by Wiley-VCH GmbH. This is an open access article under the terms of the Creative Commons Attribution Non-Commercial NoDerivs License, which permits use and distribution in any medium, provided the original work is properly cited, the use is non-commercial and no modifications or adaptations are made.

attempted a full intercalation of Mg^{2+} in TiS_2 at 100 °C with a potentiodynamic cycling procedure at C/400 in a three-electrode setup with a Mg pseudo reference electrode in 0.3 M $Mg(TFSI)_2$ in alkylcarbonates.^[19] Under these conditions, the voltage profile displayed a steep slope characteristic of a solid-solution type intercalation, which was assigned to the co-intercalation of the solvent molecules. For the solid-state electrolytes, the $Mg(BH_4)_2 \cdot 1.5THF-MgO$ (75 wt%) composite exhibited a Mg^{2+} intercalation of $x=0.2$ in Mg_xTiS_2 at C/50 on the first discharge.^[11] However, the capacity decreased rapidly in the subsequent cycles and a non-faradaic current was observed. Thus, further insight into a full battery cell and the active cathode material is required to understand the degradation and intercalation mechanism.

Here we perform a detailed structural and electrochemical investigation of an inorganic solid-state magnesium battery with layered TiS_2 as the active cathode material. The electrolyte, $Mg(BH_4)_2 \cdot 1.6NH_3-MgO$ (75 wt%), with good Mg-metal anode compatible and high Mg^{2+} conductivity is used as a solid separator in the all-solid-state batteries. Batteries assembled with two different particle sizes of TiS_2 are initially cycled galvanostatically and the cathode active material, Mg_xTiS_2 , is investigated at different stages of battery life using powder X-ray diffraction (PXD). Subsequently, a constant current constant voltage (CCCV) charging procedure is used to optimize the battery performance. The internal resistance and chemical diffusion are analyzed from galvanostatic intermittent titration technique (GITT) experiments. Our aim is to analyze the cathode structural changes during charge and discharge, and compare that to previous studies using liquid-based Mg-electrolytes.

Results and Discussion

Solid-state electrolyte pellets (50–60 mg) of $Mg(BH_4)_2 \cdot 1.6NH_3-MgO$ (75 wt%) are cast in a PEEK-die (diameter 10.3 mm and thickness of ~300 μm), and assembled as a full cell with a magnesium metal anode and layered TiS_2 as the cathode active material. The cathode active material was used as the pristine powder (TiS_2 -pristine), or as the ball-milled powder (TiS_2 -BM) with different surface areas determined by Brunauer–Emmett–Teller (BET) measurements to 2.7 or 16.5 m² g⁻¹, respectively. A catholyte mix of cathode active material, TiS_2 (75 wt%), and solid electrolyte, $Mg(BH_4)_2 \cdot 1.6NH_3$ (25 wt%), is used to obtain a suitable electronic and ionic contact, as a lower content of TiS_2 (66 wt%) or the addition of MgO nanoparticles to the catholyte mix resulted in a lower discharge capacity (Figure S1). Multiple battery cells are characterized at different stages of battery life in order to make a detailed analysis of the magnesium intercalation in the cathode active material.

The battery cells are allowed to rest for at least 24 hours at 60 °C to reach thermal and electrochemical equilibrium before cycling, which caused the open circuit voltage to decrease from 1.3 to 1.1 V (see Figures 1a, 2c, 2d and S1). In Figure 1(a), the voltage profiles during cycling between 0.2 and 1.5 V are displayed for a TiS_2 -pristine cell. The first discharge (cycle 1) resulted in a discharge capacity of 67 mAh g⁻¹, corresponding

to $\Delta x=0.14$ in Mg_xTiS_2 , and a voltage profile that displayed two distinct voltage plateaus at ~1.05 and ~0.7 V. The subsequent cycles display an increase in capacity with a maximum discharge capacity of 79 mAh g⁻¹ ($\Delta x=0.17$) and an additional voltage plateau at ~1.3 V. A previous report on the intercalation mechanism of Mg^{2+} in TiS_2 , ascribes the ~1.3, ~1.05 and ~0.7 V voltage plateaus to the phase transitions between phase 1 to 2, phase 2 to 3, and phase 3 to 4, respectively,^[18] indicating a self-discharge at the first discharge, discussed in more detail below. The charging-step is terminated prematurely on the first cycle due to a decrease in voltage at the end of charging from side reactions above the oxidative stability of the electrolyte. The voltage decrease is not observed in the following cycling, but was observed in other cells at high voltage.

The layered TiS_2 crystallizes in the trigonal space group $P-3m1$, and the two intense peaks (001) and (011) can be used to extract the a and c lattice parameters.^[20] Expansion in the a -axis corresponds to an increase within the layers, while a c -axis expansion corresponds to an increase in the interlayer distance, see Figure 1(b). Previous studies using liquid electrolytes have reported four different Mg_xTiS_2 phases during Mg^{2+} intercalation, and the same nomenclature is used here for comparison.^[18] Phase 1 corresponds to pristine TiS_2 with $a=3.40608(4)$ Å and $c=5.6977(2)$ Å, in agreement with previous reports.^[18,19,21] During discharge, phase 2 and 3 are reported, which are characterized by an expansion mainly in the interlayer distance (c -axis) assigned to Mg^{2+} occupying the octahedral sites. A composition of $Mg_{1/3}TiS_2$ is suggested for phase 3, in agreement with a stable configuration found by first-principles calculations.^[18,22] For phase 4, a noticeable expansion is observed both within the layers (a -axis) and in the interlayers (c -axis), and theoretical calculations suggests that Mg^{2+} also occupy tetrahedral sites providing higher x -values, $x>1/3$.^[22]

Battery cells at different stages of battery life are disassembled and analyzed using Rietveld refinements of PXD data in order to investigate the Mg^{2+} intercalation mechanism in TiS_2 -pristine (2.7 m² g⁻¹), see Figures 1(c) and S2. Table S1 provides an overview of the TiS_2 -pristine samples investigated by PXD. The catholyte mix is scraped off the cathode side of the battery pellets to amplify the diffraction from Mg_xTiS_2 . Therefore, some samples also contain Bragg peaks from the solid electrolyte. The cell parameters for phase 1 to 4 reported in literature are shown in Figure 1(d) as the reference values.^[18] For the as-prepared catholyte mix using TiS_2 -pristine, three distinct Mg_xTiS_2 containing phases are observed, i.e., TiS_2 in its pristine conformation, phase 1 (~75%), and two magnesium containing TiS_2 phases with an expansion along the c -axis, i.e., phase 2 (~13%) and phase 3 (~12%), revealing a spontaneous Mg^{2+} intercalation upon catholyte preparation. The as-assembled battery cell is allowed to rest for 40 hours at 60 °C (100% State-of-charge) to reach thermal equilibrium and mechanical stabilization. After resting, PXD revealed the presence of phase 1 (~33%) and phase 3 (~52%), along with a new phase with $a=3.7738(9)$ Å and $c=10.102(6)$ Å, denoted phase 5 (~16%), characterized as a significant expansion of the TiS_2 structure both in the a - and c -axis. After the 1st discharge (C/20,

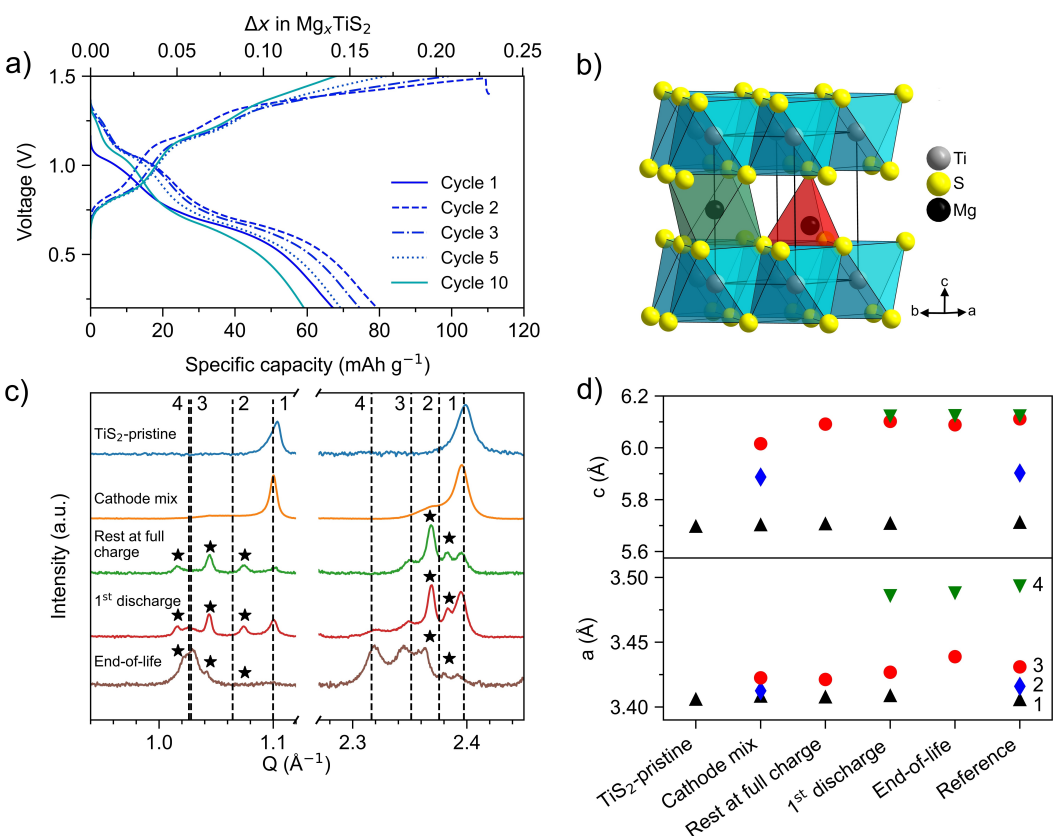


Figure 1. a) Voltage profiles at C/20 of TiS_2 -pristine ($2.7 \text{ m}^2 \text{ g}^{-1}$) at 60°C . b) Crystal structure of TiS_2 . Titanium atoms (grey) are octahedrally coordinated by sulfur atoms (yellow). Interstitial sites for Mg^{2+} are shown as octahedra (green) and tetrahedra (red). c) PXD data of battery cells at different state-of-charge of TiS_2 -pristine. Dotted lines represent TiS_2 reference phases, and (★) represent the solid electrolyte ' $Mg(BH_4)_2 \cdot 1.6NH_3$ '. d) Extracted unit cell parameters from *ex situ* PXD analysis of TiS_2 -pristine. Nomenclature of Mg_xTiS_2 phases: phase 1 (▲), phase 2 (◆), phase 3 (●), phase 4 (▼) adapted from Ref. [18].

48 mA g^{-1}) mainly phase 1 (~36%) and phase 3 (51%) are observed along with smaller amounts of the fully reduced Mg_xTiS_2 structure, phase 4 (~6%) and the more expanded phase 5 (7%). At end-of-life (C/20, 48 mA g^{-1}) using TiS_2 -pristine, i.e., upon cell failure after 59 cycles (see Figure S3), where the discharge capacity was 17% compared to the initial discharge capacity, PXD revealed the presence of phase 3 (80%), phase 4 (15%) and a minor amount of phase 5 (5%).

The PXD analysis indicates incomplete Mg^{2+} intercalation in TiS_2 -pristine, and the continued presence of phase 1 suggests that the particle core is initially unaffected, which could be a consequence of a large particle size as observed by SEM (Figure S4). This is in agreement with the previous report on Mg^{2+} intercalation in TiS_2 , where micrometer sized TiS_2 particles displayed the presence of phase 1 after discharge.^[18] The transition from phase 1 to phase 2 and to phase 3 occurs spontaneously upon catholyte mixing and cell assembly, and phase 2 changes completely to phase 3 during a 40 h resting period at 60°C . This self-discharge is also reflected in the aforementioned decrease in potential from 1.3 to 1.1 V during the resting period. The new phase observed after the resting period, phase 5, has not previously been described, but shows resemblance to co-intercalated solvent molecules observed for liquid-based electrolytes, and might be the intercalation of $[Mg(NH_3)_y]^{2+}$ complexes, resulting in a significant increase in the

TiS_2 interlayer distance. The first intense peak of phase 5 is here observed at $Q=0.6218 \text{ \AA}^{-1}$ ($d=10.10 \text{ \AA}$), suggesting a more expanded unit cell as compared to the co-intercalation reported for $Mg(TFSI)_2$ in alkylcarbonates with $Q=0.668 \text{ \AA}^{-1}$ ($d=9.406 \text{ \AA}$), and to NH_3 intercalated in TiS_2 with $Q=0.706 \text{ \AA}^{-1}$ ($d=8.91 \text{ \AA}$).^[23] However, the weak diffraction signal from phase 5 prevents detailed analysis. Phase 4 is observed after discharge to 0.2 V, consistent with additional intercalation of Mg^{2+} into the TiS_2 structure. Upon further cycling, only phase 3 and 4 and minor amounts of phase 5 are observed after 59 cycles in the end-of-life sample, suggesting that Mg^{2+} fully intercalates to the center of the larger TiS_2 particles upon extended cycling. The co-intercalation of phase 5 appears to be either reversible or occurs to a low extent, in contrast to the non-reversible solvent co-intercalation when using $Mg(TFSI)_2$ in alkylcarbonates into TiS_2 .^[19] In comparison, co-intercalation is not reported for the liquid electrolyte all-phenyl complex in THF, where reversible Mg^{2+} intercalation is reported between phase 2 and 3 to phase 4, while a non-reversible intercalation is reported from phase 1 to phase 2.^[18] However, phase 2 is not observed for the end-of-life TiS_2 -pristine sample despite a voltage profile during charging that could suggest otherwise, yet it remains unclear if this is due to a self-discharge of the cell before performing PXD or some other effects.

In order to ensure complete Mg^{2+} intercalation in the cathode active material, TiS_2 -BM with six times larger surface area ($16.5\text{ m}^2\text{ g}^{-1}$), and sub-micrometer particle size is used (Figure S4). Multiple battery cells with TiS_2 -BM are analyzed at different stages of battery life as described above, see Figures 2(a and b) and S5. An overview of the TiS_2 -BM samples investigated by PXD are provided in Table S2. In the following, the results are discussed and compared to the battery cells with TiS_2 -pristine. For the as-prepared TiS_2 -BM catholyte mix, a lower ratio of phase 1 (29%) and a higher ratio of phase 2 (22%) and phase 3 (49%) is observed. During rest (24 h at 60°C) at full charge of an assembled TiS_2 -BM cell, a higher degree of self-discharge is observed, where phase 1 (22%) and the discharged phase 3 (78%) are observed. After the 1st discharge, only the fully reduced phase 4 is observed from the combined rest and discharge steps as a result of the smaller particle size of TiS_2 . For the end-of-life sample of TiS_2 -BM, a mix of phase 3 (66%) and phase 4 (34%) is observed. Thus, cycling of the battery cell appears to be a reversible Mg^{2+} intercalation between phase 3 and phase 4. Phase 2 is not observed upon charging, in contrast to the all-phenyl complex in THF,^[18] likely due to the lower voltage cut-off at 1.2 V to avoid BH_4^- oxidation, or due to self-discharge prior to PXD measurements as discussed above.

Additionally, the new phase 5 is not observed in any of the TiS_2 -BM cells.

Initially, an attempt to cycle battery cells with TiS_2 -BM galvanostatic between 0.2 and 1.4 V resulted in fast degradation and side reactions similar to the observed voltage fluctuations described above (Figure 1a). Constant current constant voltage (CCCV) charging of TiS_2 -BM cells is implemented to circumvent the degradation and increase the performance of the cells. A TiS_2 -BM cell at C/20 with a cut-off voltage of 1.2 V displayed an increased initial discharge capacity of 112 mAh g^{-1} and $\Delta x = 0.24$ in Mg_xTiS_2 , see Figure 2(c). The following cycles have a moderate decrease in charge and discharge capacities until cycle 11, where some voltage fluctuations appear during charging. Only the two low voltage plateaus at ~ 1.05 and $\sim 0.7\text{ V}$ are present for all cycles, due to the charging cut-off voltage at 1.2 V. A TiS_2 -BM cell with a lower C-rate of C/50 displays more prominent voltage plateaus at ~ 1.05 and $\sim 0.7\text{ V}$ and an increased initial discharge capacity of 172 mAh g^{-1} ($\Delta x = 0.36$ in Mg_xTiS_2), but failed after four cycles, see Figure 2(d).

Three TiS_2 -BM cells are cycled with different cut-off voltages of 1.1, 1.2 or 1.3 V to compare the charge capacity, discharge capacity and coulombic efficiency, see Figure 3(a). The coulombic efficiencies show a clear trend from the different cut-off voltages, where a lower cut-off voltage display a higher

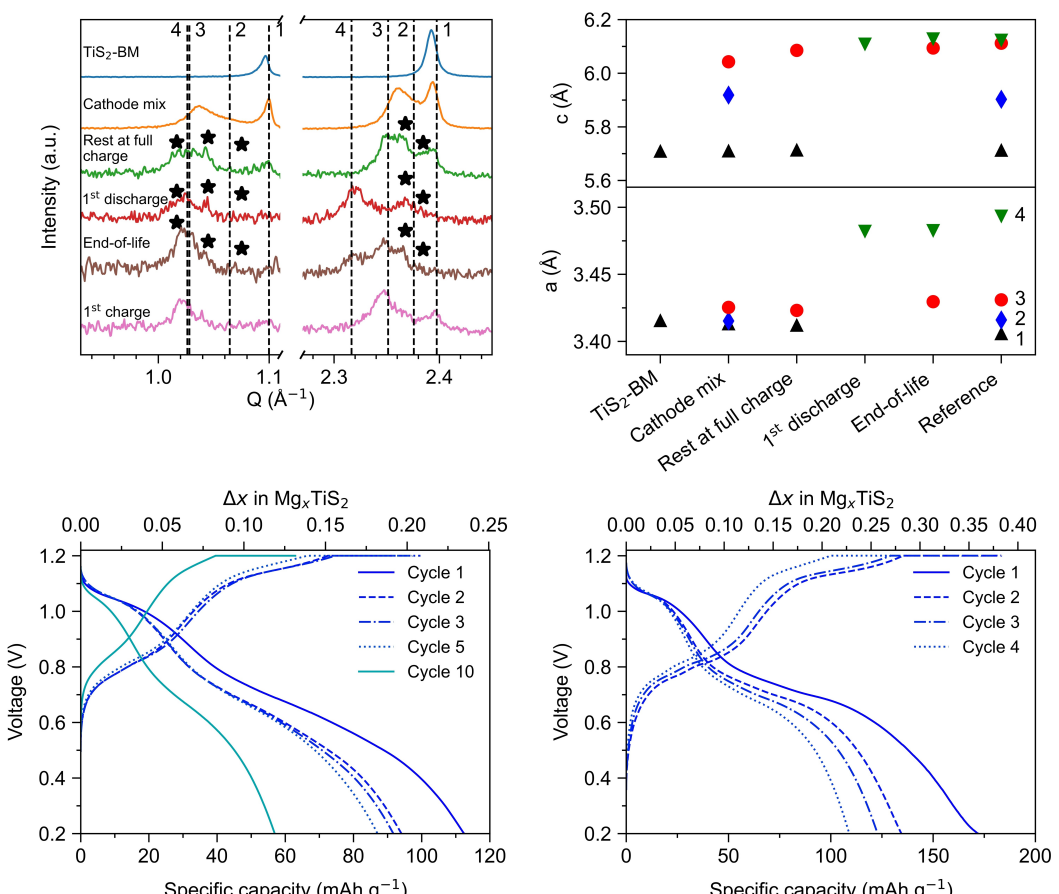


Figure 2. a) *Ex situ* PXD data of battery cells at different state-of-charge of TiS_2 -BM. Dotted lines represent TiS_2 reference phases, and (★) represent the solid electrolyte ' $Mg(BH_4)_2 \cdot 1.6NH_3$ '. b) Extracted unit cell parameters from PXD analysis of TiS_2 -BM. Nomenclature of Mg_xTiS_2 phases: phase 1 (▲), phase 2 (◆), phase 3 (●), phase 4 (▼) adapted from Ref. [18]. Voltage profiles of TiS_2 -BM ($16.5\text{ m}^2\text{ g}^{-1}$) at 60°C at c) C/20 and d) at C/50.

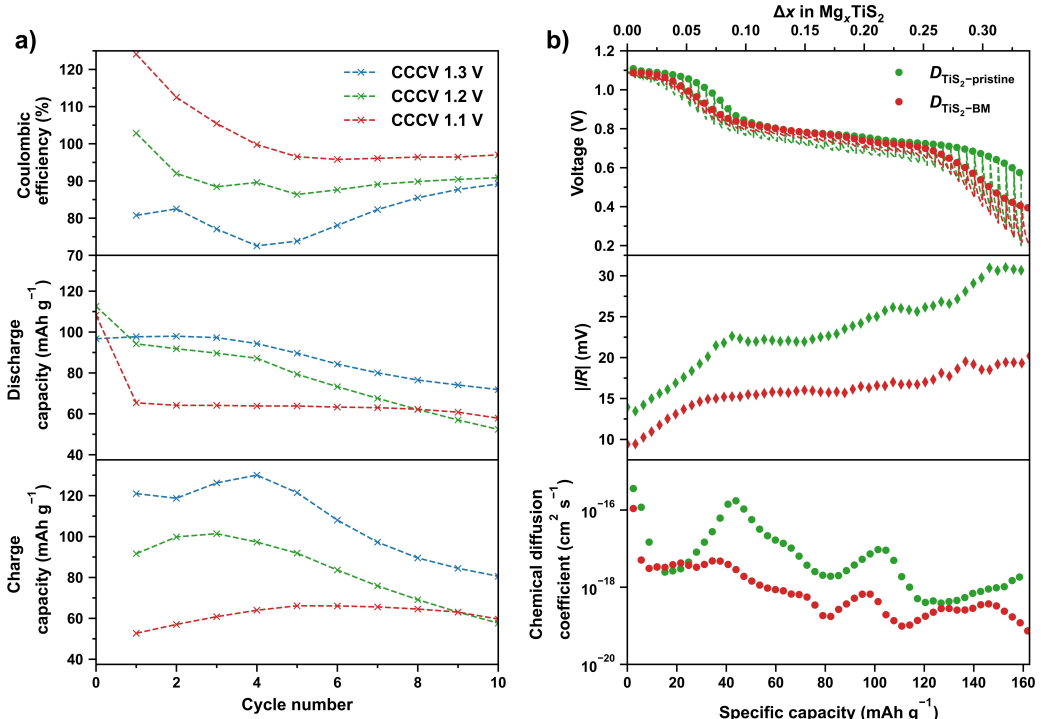


Figure 3. a) Coulombic efficiency, charge capacity and discharge capacity from utilizing a constant current constant voltage cycling of three $\text{TiS}_2\text{-BM}$ cells with a 1.1, 1.2 and 1.3 V voltage cut-off at 60 °C. b) Galvanostatic intermittent titration technique (GITT) data at C/50 with a 20 min discharging pulse and a 2 hour rest. Top) The voltage profile during the GITT experiment. Center) The $|IR|$ drop at the beginning of the charging step. Bottom) The calculated diffusion coefficients from GITT using the Weppner and Huggins equation.

efficiency. Hence, the highest coulombic efficiency is observed for a 1.1 V cut-off with an average of 105% on the first 10 cycles. For comparison, the average coulombic efficiency of cells with 1.2 and 1.3 V cut-off is 91% and 79% on the first 10 cycles, respectively. However, the high coulombic efficiency at a 1.1 V cut-off is accompanied by an insufficient capacity utilization of $\sim 70 \text{ mAh g}^{-1}$, as the cell is not fully recharged at this cut-off voltage. In addition, a coulombic efficiency above 100% may be an artifact from the large voltage relaxation after end of the discharging step, unlike the lower voltage relaxation after end of the charging step (see Figure S6). The discharge capacity gradually fade for all cells, especially at higher cut-off voltages, while the charge capacity initially increases before it begins to fade. Note that minor discrepancies in the first discharge capacity of the cells originate from small variations in the cell-assembly, but should not affect the trends in the analysis. From the relatively high capacity retention of all cells ($> 90\%$), it is evident that parasitic reactions affect the coulombic efficiency negatively. In an ideal system with an anode active material in excess, the system should be side limited to the cathode active material, i.e., where the discharge steps end due to limited accessible cathode active material sites. In this case, the coulombic efficiency should only depend on the electron current and the cathode-localized side-reaction currents (oxidation currents), which would lead to additional cyclable cations.^[24,25] However, the previous study of $\text{Mg}(\text{BH}_4)_2 \cdot 1.6\text{NH}_3\text{-MgO}$ (75 wt%) displayed the initial formation of an interface towards magnesium metal before stable cycling in

a symmetric magnesium cell.^[10] In addition, the incomplete intercalation observed from the PXD analysis suggests sluggish kinetics in the cathode active material, which leads to a large polarization and premature termination of the discharge steps. Despite these exceptions, the oxidation of the electrolyte, especially above 1.2 V vs. Mg/Mg^{2+} , is continuous and occurs at a higher rate at higher potentials, which leads to faster battery failure.

Galvanostatic intermittent titration technique (GITT) experiments are conducted to obtain insight into the diffusion processes and resistances in the solid-state cells with TiS_2 -pristine and $\text{TiS}_2\text{-BM}$ cathodes, see Figure 3(b). The cells are perturbed in pulses of 20 min with 9.6 mA g^{-1} (C/50) and allowed to rest for 2 hours. The voltage profiles and open circuit voltage at the end of the rest step as a function of state-of-charge of the TiS_2 -pristine and $\text{TiS}_2\text{-BM}$ cells display similar plateaus for both cells (Figure 3b top). The voltage of $\text{TiS}_2\text{-BM}$ drops faster to the 0.7 V plateau compared to TiS_2 -pristine, which is consistent with the higher degree of self-discharge observed from the PXD analysis. The voltage changes throughout the discharges are consistently larger for the TiS_2 -pristine cell. The $|IR|$ drop of the TiS_2 -pristine and the $\text{TiS}_2\text{-BM}$ cells reveal a lower internal resistance on the $\text{TiS}_2\text{-BM}$ cell (Figure 3b center). For both the TiS_2 -pristine and the $\text{TiS}_2\text{-BM}$ cell, the $|IR|$ drop increases more on the initial pulses, and less when it reaches the 0.7 V plateau. The internal resistance is often constant in a battery, so a change in resistance is likely from an oxidation of the solid electrolyte at the cathode side, interface

formation at the anode side, or from contact loss associated with Mg stripping or TiS_2 volume-changes. The chemical diffusion coefficient, D_{Mg}^{2+} , has been calculated according to Weppner and Huggins equation (Equation 1) from the voltage changes of a current pulse (Figure 3b bottom). Note that GITT is measured under non-ideal conditions, as the measurement is performed in a two-electrode setup with a non-ideal counter/reference electrode, thus will be influenced by the anode, the solid electrolyte, the interfaces and the cathode migration barriers. Therefore, the analysis here is limited to the entire cell and not only the chemical diffusion in the active material as usually investigated with this technique. In both cells, the chemical diffusion coefficient is in the order of 10^{-15} to $10^{-19} \text{ cm}^2 \text{s}^{-1}$ and is generally increasing on the voltage slopes. As the entire cell is probed, the difference between the TiS_2 -pristine and the TiS_2 -BM cell is from the larger amount of formed interface on the smaller TiS_2 -BM particles, resulting in a lower chemical diffusion coefficient at higher state-of-charge. In comparison, the commonly used magnesium cathode, Mo_6S_8 Chevrel phase and the spinel-type Ti_2S_4 , have chemical diffusion coefficients around $\sim 10^{-12} \text{ cm}^2 \text{s}^{-1}$, which are more ideal for battery materials.^[26,27] The low chemical diffusion coefficient at elevated temperatures found in this study is similarly in agreement with a relatively high Mg^{2+} migration barrier of $> 1 \text{ eV}$ calculated in a computational study on layered TiS_2 .^[22]

Conclusions

In summary, we investigated the utilization of layered titanium disulfide, TiS_2 , as an intercalation cathode active material for all-solid-state magnesium batteries, using a nanocomposite electrolyte, $\text{Mg}(\text{BH}_4)_2 \cdot 1.6\text{NH}_3\text{-MgO}$ (75 wt%), and Mg-metal as the anode active material. This has resulted in the best performing inorganic solid-state magnesium battery reported so far, and a high discharge capacity of 172 mAh g^{-1} is achieved at C/50. Our findings demonstrate that the electrolyte, $\text{Mg}(\text{BH}_4)_2 \cdot 1.6\text{NH}_3$, reacts with TiS_2 (phase 1), resulting in self-discharged Mg_xTiS_2 (phase 2) already upon mixing, and a further discharged state upon full-cell assembly (phase 2 and 3). During charge and discharge, Mg is reversibly intercalated into Mg_xTiS_2 , cycling between phase 3 (charged) and phase 4 (discharged). The pristine micrometer-sized TiS_2 prevented full intercalation, while ball milling resulted in sub-micrometer sized TiS_2 , allowing for faster kinetics, but also resulting in a higher extent of self-discharge in the catholyte mix. Parasitic reactions are observed at $> 1.2 \text{ V}$, and constant current constant voltage charging is utilized to limit the degradation and increase the performance of the cells. Finally, galvanostatic intermittent titration technique experiments are used to determine the chemical diffusion coefficient of the entire cell, which is in the order of 10^{-15} to $10^{-19} \text{ cm}^2 \text{s}^{-1}$. Future research should focus on expanding the oxidative stability of the electrolyte to prevent self-discharge and electrolyte decomposition. Possible solutions may include the formation of a stable interface layer or coating of the cathode active material, similar to what is being explored for thiophosphate- and argyrodite-based Li-electrolytes.^[28-30] Alter-

natively, cathode active materials such as Mo_6S_8 Chevrel phase or spinel-type Ti_2S_4 show higher chemical magnesium diffusion coefficients, and can be investigated as potential cathodes.

Experimental Section

Synthesis

The solid-state electrolyte, $\text{Mg}(\text{BH}_4)_2 \cdot 1.6\text{NH}_3$, was synthesized mechanochemically by mixing $\alpha\text{-Mg}(\text{BH}_4)_2$ and $\text{Mg}(\text{BH}_4)_2 \cdot 6\text{NH}_3$ in a stoichiometric ratio as described previously in the literature.^[10] For the electrolyte separator layer, $\text{Mg}(\text{BH}_4)_2 \cdot 1.6\text{NH}_3\text{-MgO}$ (75 wt%), 75 wt% MgO ($\sim 50 \text{ nm}$) was added to $\text{Mg}(\text{BH}_4)_2 \cdot 1.6\text{NH}_3$ by mechanochemical treatment. The powders were loaded in an 80 mL WC coated steel vial and WC balls (5.5 g each) with a ball-to-powder weight ratio of 30:1. The ball-milling program was 200 rpm for 2 min, followed by a 2 min pause with 90 repetitions.

Cell assembly

The cathode active material, titanium disulfide (99.9%, Sigma-Aldrich), was used as received (TiS_2 -pristine) or as a ball-milled powder (TiS_2 -BM), obtained by a ball-milling program of 450 rpm for 2 min, followed by a 2 min pause with 29 repetitions. The surface area of the powders was determined by Brunauer–Emmett–Teller measurements.

The catholyte, comprised of either TiS_2 -pristine or TiS_2 -BM, and $\text{Mg}(\text{BH}_4)_2 \cdot 1.6\text{NH}_3$, was hand grinded for 10 min in a weight ratio of 75:25 of the respective compounds. Battery cells were assembled in in-house built polyetheretherketone (PEEK) cells at room temperature. An Mg electrode (99.9%, Alfa Aesar) was hand-polished with SiC paper and loaded into the PEEK cell. A powder loading of the electrolyte $\text{Mg}(\text{BH}_4)_2 \cdot 1.6\text{NH}_3\text{-MgO}$ (50–60 mg) was added to the cell and an electrolyte separator pellet was cast directly in the 10.3 mm PEEK-die at 235 MPa. The resulting pellets were between 300–400 μm in thickness. Catholyte (2–4 mg) was loaded on the pellet and prepressed before a Mo current collector was added and pressed at 350 MPa for 1 min.

X-ray diffraction

In-house powder X-ray diffraction (PXD) was collected on a Rigaku SmartLab diffractometer with a Cu anode ($\text{Cu K}\alpha_1$ radiation, 2 kW, $\lambda = 1.54056 \text{ \AA}$) at room temperature. Synchrotron radiation powder X-ray diffraction (SR-PXD) data were collected at the Diamond Light Source at beamline I11 using $\lambda = 0.826927 \text{ \AA}$. All samples were loaded in 0.5 mm borosilicate capillaries and sealed in argon atmosphere. Structural refinements were performed in the software FullProf using the crystal structural models of $\text{Mg}(\text{BH}_4)_2 \cdot 1\text{NH}_3$, $\text{Mg}(\text{BH}_4)_2 \cdot 2\text{NH}_3$ and TiS_2 .^[31] The background was described by linear interpolation between selected points, while Pseudo-Voigt profile functions were used to fit the diffraction peaks. As the exact crystal structures of Mg_xTiS_2 (phase 2, 3, 4 and 5) are unknown, the structure of TiS_2 was used to fit these phases to extract the cell parameters and the relative content of the individual phases.

Electrochemistry

All electrochemical measurements were conducted with a Biologic SP-300 in a Memmert Climate chamber at 60°C . The stack pressure was initially set to $\sim 25 \text{ MPa}$ before allowing all cells to reach

thermal equilibrium at 60 °C for 24 hours, unless otherwise specified.

Galvanostatic cycling was performed with a lower and upper limit of 0.2 and 1.5 V, respectively. Constant current constant voltage (CCCV) charging of TiS₂-BM cells was charged with a constant current until the cut-off voltage was reached and held at the cut-off voltage until a current of 25% of the initial charging current was reached.

Galvanostatic intermittent titration technique (GITT) experiments were performed in two-electrode cells as described above. Current pulses of 9.6 mA g⁻¹ (C/50) were applied for 20 min, and allowed to rest for 2 hours afterwards. The IR drop was estimated from the voltage decrease on the first 10 s after perturbation, and the diffusion coefficient ($D_{\text{Mg}^{2+}}$) is calculated according to Eq. (1):^[32]

$$D_{\text{Mg}^{2+}} = \frac{4}{\pi} \left(\frac{m_{\text{CAM}} V_m}{M_{\text{CAM}} A_s} \right)^2 \left(\frac{\Delta E_s}{\tau \left(\frac{dE}{dt} \right)} \right)^2 \quad (1)$$

where m_{CAM} is the mass of the cathode active material, V_m is the molar volume, M_{CAM} is the atomic weight, A_s is the surface area exposed to electrolyte (considered as fully covered), ΔE_s is the change of the steady-state voltage before and after the pulse, $dE/d\sqrt{t}$ is the slope during the pulse and τ is the pulse duration.

Supporting Information

Supporting Information is available from the Wiley Online Library or from the author.

Acknowledgements

The work was supported by the Danish Council for Independent Research (SOS-MagBat DFF9041-00226B and CaMBat DFF0217-00327B). Affiliation with the Center for Integrated Materials Research (iMAT) at Aarhus University is gratefully acknowledged. The Carlsberg Foundation is acknowledged for funding the Tescan Clara SEM used in this work. We also thank beamline I11 at the Diamond Light Source for provision of beamtime and the local contacts Stephen Thompson and Eamonn Connolly for assistance with data collection.

Conflict of Interests

The authors declare no conflict of interest.

Data Availability Statement

The data that support the findings of this study are available in the supplementary material of this article.

Keywords: magnesium titanium disulfide • magnesium cathode • magnesium metal anode • solid-state magnesium batteries

- [1] M. Fichtner, Ed., *Magnesium Batteries: Research and Applications*, The Royal Society of Chemistry, 2020.
- [2] T. D. Tran, J. H. Feikert, X. Song, K. Kinoshita, *J. Electrochem. Soc.* **1995**, 142, 3297.
- [3] J. Asenbauer, T. Eisenmann, M. Kuenzel, A. Kazzazi, Z. Chen, D. Bresser, *Sustain. Energy Fuels* **2020**, 4, 5387.
- [4] R. Davidson, A. Verma, D. Santos, F. Hao, C. D. Fincher, D. Zhao, V. Attari, P. Schofield, J. Van Buskirk, A. Fraticelli-Cartagena, T. E. G. Alivio, R. Arroyave, K. Xie, M. Pharr, P. P. Mukherjee, S. Banerjee, *Mater. Horiz.* **2020**, 7, 843.
- [5] M. Guo, C. Yuan, T. Zhang, X. Yu, *Small* **2022**, 18, 2106981.
- [6] Z. Rong, R. Malik, P. Canepa, G. Sai Gautam, M. Liu, A. Jain, K. Persson, G. Ceder, *Chem. Mater.* **2015**, 27, 6016.
- [7] J. B. Grinderslev, M. B. Amdisen, L. N. Skov, K. T. Møller, L. G. Kristensen, M. Polanski, M. Heere, T. R. Jensen, *J. Alloys Compd.* **2021**, 163014.
- [8] F. Cuevas, M. B. Amdisen, M. Baricco, C. E. Buckley, Y. W. Cho, P. de Jongh, L. M. de Kort, J. B. Grinderslev, V. Gulino, B. C. Hauback, M. Heere, T. Humphries, T. R. Jensen, S. Kim, K. Kisu, Y.-S. Lee, H.-W. Li, R. Mohitadi, K. T. Møller, P. Ngene, D. Noréus, S. Orimo, M. Paskevicius, M. Polanski, S. Sartori, L. N. Skov, M. H. Sørby, B. C. Wood, V. A. Yartys, M. Zhu, M. Latroche, *Prog. Energy* **2022**, 4, 032001.
- [9] L. G. Kristensen, M. B. Amdisen, L. N. Skov, T. R. Jensen, *Phys. Chem. Chem. Phys.* **2022**, 24, 18185.
- [10] Y. Yan, J. B. Grinderslev, M. Jørgensen, L. N. Skov, J. Skibsted, T. R. Jensen, *ACS Appl. Energ. Mater.* **2020**, 3, 9264.
- [11] L. N. Skov, J. B. Grinderslev, A. Rosenkrantz, Y.-S. Lee, T. R. Jensen, *Batteries & Supercaps* **2022**, 5, e202200163.
- [12] Y. Yan, W. Dononelli, M. Jørgensen, J. B. Grinderslev, Y.-S. Lee, Y. W. Cho, R. Černý, B. Hammer, T. R. Jensen, *Phys. Chem. Chem. Phys.* **2020**, 22, 9204.
- [13] L. G. Kristensen, M. B. Amdisen, M. Andersen, T. R. Jensen, *Inorganics* **2022**, 11, 17.
- [14] M. S. Whittingham, *Chem. Rev.* **2004**, 104, 4271.
- [15] H. Wan, S. Liu, T. Deng, J. Xu, J. Zhang, X. He, X. Ji, X. Yao, C. Wang, *ACS Energy Lett.* **2021**, 6, 862.
- [16] W. Weng, G. Liu, Y. Li, L. Shen, X. Yao, *Appl. Mater. Today* **2022**, 27, 101448.
- [17] V. Gulino, M. Brighi, F. Murgia, P. Ngene, P. De Jongh, R. Černý, M. Baricco, *ACS Appl. Energ. Mater.* **2021**, 4, 1228.
- [18] X. Sun, P. Bonnick, L. F. Nazar, *ACS Energy Lett.* **2016**, 1, 297.
- [19] D. S. Tchitchevka, A. Ponrouch, R. Verrelli, T. Broux, C. Frontera, A. Sorrentino, F. Bardé, N. Biskup, M. E. Arroyo-de Dompablo, M. R. Palacín, *Chem. Mater.* **2018**, 30, 847.
- [20] M. J. McKelvy, W. S. Glaunsinger, *J. Solid State Chem.* **1987**, 66, 181.
- [21] J. Bear, F. K. McTaggart, *Aust. J. Chem.* **1958**, 11, 458.
- [22] A. Emly, A. Van der Ven, *Inorg. Chem.* **2015**, 54, 4394.
- [23] R. R. Chianelli, J. C. Scanlon, M. S. Whittingham, F. R. Gamble, *Inorg. Chem.* **1975**, 14, 1691.
- [24] A. Tornheim, D. C. O'Hanlon, *J. Electrochem. Soc.* **2020**, 167, 110520.
- [25] A. J. Smith, J. C. Burns, D. Xiong, J. R. Dahn, *J. Electrochem. Soc.* **2011**, 158, A1136.
- [26] M. D. Levi, E. Lancry, H. Gizbar, Y. Gofer, E. Levi, D. Aurbach, *Electrochim. Acta* **2004**.
- [27] X. Sun, P. Bonnick, V. Duffort, M. Liu, Z. Rong, K. A. Persson, G. Ceder, L. F. Nazar, *Energy Environ. Sci.* **2016**, 9, 2273.
- [28] L. M. Rieger, R. Schlem, J. Sann, W. G. Zeier, J. Janek, *Angew. Chem. Int. Ed.* **2021**, 60, 6718.
- [29] T. Famprakis, P. Canepa, J. A. Dawson, M. S. Islam, C. Masquelier, *Nat. Mater.* **2019**, 18, 1278.
- [30] Y. Lee, J. Jeong, H. J. Lee, M. Kim, D. Han, H. Kim, J. M. Yuk, K.-W. Nam, K. Y. Chung, H.-G. Jung, S. Yu, *ACS Energy Lett.* **2022**, 7, 171.
- [31] J. R. Carvajal, *LLB Sacré & LCSM Rennes, France* n.d., 2003.
- [32] W. Weppner, R. A. Huggins, *J. Electrochem. Soc.* **1977**, 124, 1569.

Manuscript received: May 3, 2023

Revised manuscript received: June 6, 2023

Accepted manuscript online: June 7, 2023

Version of record online: June 29, 2023